Analysis of the singular vectors of the full-physics Florida State University Global Spectral Model

By ZHIJIN LI[1]†, I. M. NAVON[2]* and M. Y. HUSSAINI[1],   [1]*School of Computational Science and Information Technology, Florida State University, Tallahassee, FL 32306, USA;* [2]*Department of Mathematics and School of Computational Science and Information Technology, Florida State University, Tallahassee, FL 32306, USA*

ABSTRACT

Analysis of singular vectors (SVs) is performed on the Florida State University Global Spectral Model, which includes linearized full physics of the atmosphere. It is demonstrated that the physical processes, especially precipitation, fundamentally affect the leading SVs. When the SVs are coupled with the precipitation geographically, their growth rates increase substantially and their structures change significantly. The physical processes however have little impact on growth rates or structures of the SVs that are geographically independent of precipitation. Furthermore, it is shown that spatial filtering along with the projection operator that projects the flow winds to the rotational wind (designed as a simple initialization process) improves the structural features of SVs and is found to mitigate spurious modes.

1. Introduction

In the 1960s, Lorenz (1965) introduced singular vector (SV) analysis in meteorology to compute the largest error growth rates and to estimate the atmospheric predictability of an idealized model. However, SV analysis was carried out for the realistic meteorological problems only in the late 1980s, a major obstacle being the huge computational expense. At the beginning of the 1990s, with the advent of adjoint techniques for the computation of SVs in meteorological problems (Molteni and Palmer, 1993; Mureau et al., 1993), the SV analysis for the sophisticated atmospheric general circulation models (GCMs) became feasible. SV analysis has since found applications in the areas of initial conditions for ensemble forecasting (Mureau et al., 1993; Molteni et al., 1996), of error-growth estimation in numerical weather prediction and atmospheric predictability (Molteni and Palmer, 1993; Ehrendorfer and Tribbia, 1997) and of adaptive observation strategy for ensemble forecasting (Gelaro et al., 1998; Lorenz and Emanuel, 1998; Palmer et al., 1998; Buizza and Montani, 1999; Puri et al., 2001). Thus, the SV analysis has become as commonplace as normal mode analysis in the study of atmospheric flow instability (e.g. Farrell, 1988, 1989; Borges and Hartmann, 1992; Molteni and Palmer, 1993; Li and Ji, 1996, 1997; de Pondeca et al., 1998; Oortwijn, 1998). Even

so, the most successful application of SV analysis appears to be in generating the initial conditions for ensemble forecasts (see Toth and Kalnay, 1997).

The SV analysis for the numerical weather prediction models has been the subject of numerous studies. For the barotropic atmosphere, there are investigations by Borges and Hartmann (1992), Molteni and Palmer (1993) and Li and Ji (1996, 1997), to mention a few. The European Centre for Medium-Range Weather Forecasts (ECMWF) has investigated the impact of model physics, resolution and atmospheric states on the feature of SVs for the atmospheric GCM of ECMWF (Buizza, 1994; Buizza and Palmer, 1995; Buizza and Montani, 1999; Mahfouf, 1999; Barkmeijer et al., 2001; Puri et al., 2001). Also, the National Center for Atmospheric Research (NCAR) has examined the influence of moist physics on the SVs in the mesoscale model NCAR MM4 (Ehrendorfer et al., 1999). The research efforts at both ECMWF and NCAR have shown that the physical processes, in particular the boundary layer and moist physics, have a substantial impact on SVs. As the physical parametrization dramatically differs among different GCMs (while the dynamical part is generally similar), further examination of such observations in the framework of other models is warranted. The objective of our present work is to study this problem in the context of the Florida State University Global Spectral Model (FSUGSM), which has been used in numerical weather prediction for operational purposes for more than a decade. This model incorporates the physics of tropical meteorology.

As the SVs are computed by optimizing the growth of linear perturbations of the state trajectory, a persistent problem is

---

*Corresponding author.
e-mail: navon@csit.fsu.edu
†Present address: Jet Propulsion Laboratory, California Institute of Technology, Pasadena, CA 91109, USA.

the appearance of spurious modes. Buizza (1994) was the first to notice that such modes existed near and within the planetary boundary layer and decayed fast during the integration of the non-linear model. He called them non-meteorological modes and he suggested that the introduction of boundary-layer physics into the linearized model should suppress them. Barkmeijer et al. (2001) also observed similar modes in the tropical upper troposphere and showed that they were inertia waves that grew only in the linearized model. These spurious modes are distinct from known meteorological modes. We observe that the linearization can also lead to a spuriously large growth rate and a spuriously distorted structure of the leading SVs, even though they essentially consist of meteorological modes. This is a significant issue for predictability estimation and ensemble forecasting. Mitigation of the spurious effect of linearization on leading SVs is the key issue addressed in this work.

There are essentially two ways one could deal with the spurious modes. In the first approach, one adjusts the physical model parameters or modifies model physics. Such an approach was adopted by Buizza (1994) and Barkmeijer et al. (2001), who introduced boundary-layer physics and increased the value of the dissipation parameters in the vertical direction. In the second approach, one projects the variables used to compute the SVs on to a subspace that excludes spuriously growing modes. For example, one projects the wind velocity on to the rotational component; in other words, the divergent component of wind velocity is suppressed (Errico, 2000a,b). In view of the fact that spurious modes are localized at specific vertical model levels, Barkmeijer et al. (2001) noted the possibility of suppressing these modes by defining the variables for the computation of SVs on the model levels excluding those where the spurious modes appear.

A physically sound method for suppressing spurious modes is to introduce an initialization procedure that filters out the spuriously growing modes in the initial conditions (Haltiner and Williams, 1980). However, an operational initialization procedure is computationally demanding and hence could not be used directly in the computation of SVs, which requires multiple iterations. One may conjecture that to suppress spurious modes would require design of a filter that has the advantageous feature of an initialization procedure while allowing efficient computation. However, the experience of Montani and Thorpe (2002) shows that this does not prevent the SVs from having unbalanced features. We propose a generalized filter that is a product of the projection operator of Barkmeijer (which projects on to a specified area) and a filter operator (which filters out either spatial scales or temporal scales or both, thereby mitigating or precluding spurious modes). Spatial filters have been used to investigate the effect of spatial scales on the linear growth rate of SVs (Hartmann et al., 1995) as well as balance constraints. Such a filter operator can also be identified with the projection operator of Errico (2000a,b) that projects the wind velocity field on to its rotational component. We show in this work that combining a low pass filter (which suppresses high wavenumbers) with some

balance constraints effectively suppresses spurious modes, and more importantly improves the features of computed SVs.

Another aspect is related to the scheme of convective parametrization used in our experiments, i.e. the modified Kuo (1974) scheme instead of the relaxed Arakawa and Schubert (1974) scheme (see Moorthi and Suarez, 1992) used in similar studies.

Hansen and Smith (2000) point out that in the presence of model error, the usefulness of SVs for adaptive observations is limited to the case when the linearity assumption as mentioned in their paper is valid (i.e. model linearization about the analysis requires the analysis error to be sufficiently small). In particular, section 3 of their paper is relevant. Liu and Navon (2002) carried out such a careful verification.

The issue about successful application of SVs in general and the above-mentioned issues raised in Smith (2000) and Hansen and Smith (2000), related to explicitly accounting for the dynamical evolution of uncertainty, are valid issues and depend on the relative magnitude of operational analysis errors.

A recent work by Coutinho et al. (2004) presents a slightly different perception about the impact of the inclusion of a full linearized physical parametrization package on extratropical SVs using the ECMWF integrated forecasting system. The crucial ingredient in the full package turns out to be the large-scale latent heat release. Some of the moist SVs occur at new locations and have tighter structures.

This paper is organized as follows. After this general introduction, the FSUGSM and its linearization are briefly described in Section 2. A basic derivation of the general expressions for computations of SVs is presented in Section 3. The impact of physical processes on SVs is discussed in Section 4. The application of the generalized filter is described in Section 5. Finally, key results are discussed and summarized in Section 6.

2. Basic formulation of singular vector decomposition

For the sake of completeness, a brief description of the FSUGSM is provided along with a succinct discussion of the SV decomposition.

2.1. Global spectral model

The FSUGSM has been used in operational weather forecasts for more than a decade. Forecasts based on this model emphasize tropical aspects such as monsoons and tropical storms (e.g. Krishnamurti et al., 1991). This model has a comprehensive advanced physical parametrization package. The main physical parametrizations include a fourth-order horizontal diffusion (Kanamitsu et al., 1983), a modified Kuo-type convective scheme (Krishnamurti et al., 1993), dry convective adjustment, large-scale condensation, surface flux via similarity theory (Businger et al., 1971), vertical distribution of fluxes utilizing diffusive formulation where the exchange coefficients are functions of the

Richardson number (Louis, 1979), long-wave and short-wave radiative fluxes based on a band model (Harshvardan and Corsetti, 1984; Lacis and Hansen, 1974), computation of low, middle and high clouds based on threshold relative humidity for radiative calculation and surface energy balance coupled to the similarity theory (Krishnamurti et al., 1991).

The adjoint system of the FSUGSM is a result of several years effort. The adjoint system includes the dynamic core (Wang, 1993) and all above-mentioned physical parametrizations (Tsuyuki, 1996; Zhu and Navon, 1997). Both the tangent linear model and consequently the adjoint contain simplifications with respect to the non-linear forecast model. This model has been successfully applied to carry out both 4D-Var and optimal parameter estimation (Tsuyuki, 1997; Zhu and Navon, 1999; Li et al., 2000).

In the following computations, the spectral expansion of the model variables is triangularly truncated at the wavenumber 42 (T42). A sigma (σ) coordinate is used in the vertical direction and the vertical resolution consists of 12 layers roughly between 100 and 1000 hPa.

2.2. Singular value decomposition basics

Consider the FSUGSM, which is perturbed at any point in its non-linear trajectory. The evolution of the perturbation state vector x is then governed by

$$x_t = A(t, 0)x_0, \tag{1}$$

where x_t is the perturbation at time t, x_0 is the initial perturbation at time 0, and $A(t, 0)$ is the resolvent or forward tangent propagator from time 0 to time t. $A(t, 0)$ is a linearized version of the original non-linear operator. Equation (1) is usually called the tangent linear model. In the present case, the perturbation state vector x represents $\{u, v, T, \ln \pi\}$, which are the perturbations of velocity components, temperature, and logarithm of surface pressure, respectively.

In order to compute the fastest growing perturbations (the so-called SVs that will be defined precisely later), it is necessary to define an inner product for the linear vector space of perturbations. We define the inner product, $(x, y) = \langle x, Ey \rangle$, where $\langle . ; . \rangle$ denotes a Euclidean scalar product and E denotes a weight matrix, so that it yields the norm

$$||x||^2 = (x, x) = \langle x, Ex \rangle = \frac{1}{2} \int_0^1 \int_\Sigma \left[u^2 + v^2 + \frac{c_p}{T_r} T^2 \right]$$
$$\times \left(\frac{\partial p}{\partial \sigma} \right) d\Sigma \, d\sigma + \frac{1}{2} \int_\Sigma R_d T_r P_r (\ln \pi)^2 \, d\Sigma. \tag{2}$$

Here, C_p is the specific heat of dry air at constant pressure, R_d is the gas constant for dry air, $T_r = 300$ K is a reference temperature, and $P_r = 800$ hpa is a reference pressure. E is obviously a positive-definite diagonal matrix. This norm (2) does not include the latent heat of condensation (Mahfouf et al., 1996; Ehrendorfer et al., 1999) and is called the dry total energy norm. As pointed out by Buizza and Palmer (1995), such a norm per-

mits reverse energy cascade from subsynoptic to synoptic scales. Molteni et al. (1996) observe that, in the absence of complete analysis-error covariance, the total energy norm is the most appropriate for ensemble prediction. Its physical relevance and importance are due to the fact that it includes kinetic, thermal and potential energies. We did not include moisture in the norm as there is at present a certain arbitrariness in modeling specific humidity (Mahfouf et al., 1996).

In the discrete case pertaining to the FSUGSM under study, the perturbation state vector $x = \{u, v, T, \ln \pi\}$ is of dimension $M = I * J * (3K + 1)$ where I, J, and K are the number of degrees of freedom in the longitudinal (i), latitudinal (j), and vertical (k) directions. The matrix A is $M * M$, real and non-singular. The matrix E in the weighted inner product is diagonal, positive-definite and it has the form

$$\mathbf{E} = \text{diag}\Big\{ \cdots, w(j)p_s(i, j)\delta\sigma(k)\delta\lambda, \cdots, \cdots, w(j)p_s(i, j)$$
$$\times \delta\sigma(k)\delta\lambda, \cdots, \cdots, w(j)p_s(i, j)\frac{c_p}{T_r}$$
$$\times \delta\sigma(k)\delta\lambda, \cdots, \cdots, w(j)R_d T_r P_r \delta\lambda, \cdots \Big\}, \tag{3}$$

where $\delta\lambda$ and $\delta\sigma$ (k) are the step sizes in the longitude and vertical directions, respectively, and $p_s(i, j)$ is the surface pressure. The Gaussian integration is used in latitude, and $w(j)$ are the Gaussian weights.

The definition of the norm allows us to relate the energy of the perturbation x at time t to its initial value

$$\frac{||x_t||^2}{||x_0||^2} = \frac{\langle x_t, E_t x_t \rangle}{\langle x_0, E_0 x_0 \rangle} = \frac{\langle Ax_0, E_t Ax_0 \rangle}{\langle x_0, E_0 x_0 \rangle}$$
$$= \frac{\langle x_0, A^T E_t Ax_0 \rangle}{\langle x_0, E_0 x_0 \rangle} = \lambda^2, \tag{4}$$

where the superscript 'T' represents the transpose, and the subscripts t and 0 denote the weight matrix at time t and 0. In the present instance, $E_t = E_0$ and λ is usually called the energy amplification factor.

This suggests the generalized eigenvalue problem

$$A^T E_t A v_i = \lambda_i^2 E_0 v_i. \tag{5}$$

$A^T E_t A$ is symmetric and positive-definite and its eigenvalues can be ranked in the decreasing order: $\lambda_1 > \lambda_2 > \lambda_3 > \cdots > \cdots > 0$. The generalized eigenvectors v_i and the generalized eigenvalues λ_i are respectively called the SVs and singular values of A (with respect to E_0 norm). They are orthogonal and form a complete basis. Any x_t can therefore be expressed as a linear combination of the SVs v_i, and the amplification factor as a linear combination of the singular values λ_i. The leading SVs are sometimes called optimal perturbations and the time during which perturbation growth is considered the optimization time.

In practice, one can only compute a small number of SVs compared with the huge dimension of the model variables. In order to make the SVs more relevant to limited area models, Barkmeijer (1992) introduced a local projection operator P, which sets model variables to zero outside the concerned area.

Then the definition of the amplification factor (4) is generalized as

$$\lambda^2 = \frac{\langle Px_t, E_t Px_t \rangle}{\langle x_0, E_0 x_0 \rangle}. \tag{6}$$

This projection operator has been used extensively in SV analysis (e.g. Barkmeijer, 1992; Buizza et al., 1997). Pursuing this line of argument, one can further introduce a filter operator F and generalize eq. (6) as

$$\lambda^2 = \frac{\langle P F_t x_t, E_t P F_t x_t \rangle}{\langle F_0 x_0, E_0 F_0 x_0 \rangle}. \tag{7}$$

If F_t and F_0 transform the complete wind field to the rotational field (i.e. filters out the potential component), they could be identified with the projection operator discussed by Errico (2000a,b). In the following computations, F will be a temporal or spatial filter combined with other constraints, aimed at suppressing spurious modes in leading SVs and at improving their features.

Consistent with the generalized definition of amplification factor (7), the eigenvalue problem becomes

$$A^T F_t^T P^T E_t P F_t A v = \lambda^2 F_0^T E_0 F_0 v. \tag{8}$$

Obviously, $A^T F_t^T P^T E_t P F_t A$ and $F_0^T E_0 F_0$ are positive semi-definite matrices. The SVs and singular values have the same properties as those for the definition (4), but SVs are orthonormal and complete with respect to $F_0^T E_0 F_0$.

When the adjoint operators A^T, F^T, and P^T are available, the eigenvalue problem (8) can be solved even for a sophisticated GCM by using Lanczos-type algorithms. These algorithms require only the evaluation of matrix–vector products and circumvent the computationally expensive explicit manipulations of those large matrices. There are quite a few software packages based on Lanczos-type algorithms. We use the ARPACK software package that was developed specifically for problems of large dimensions (Lehoucq et al., 1998).
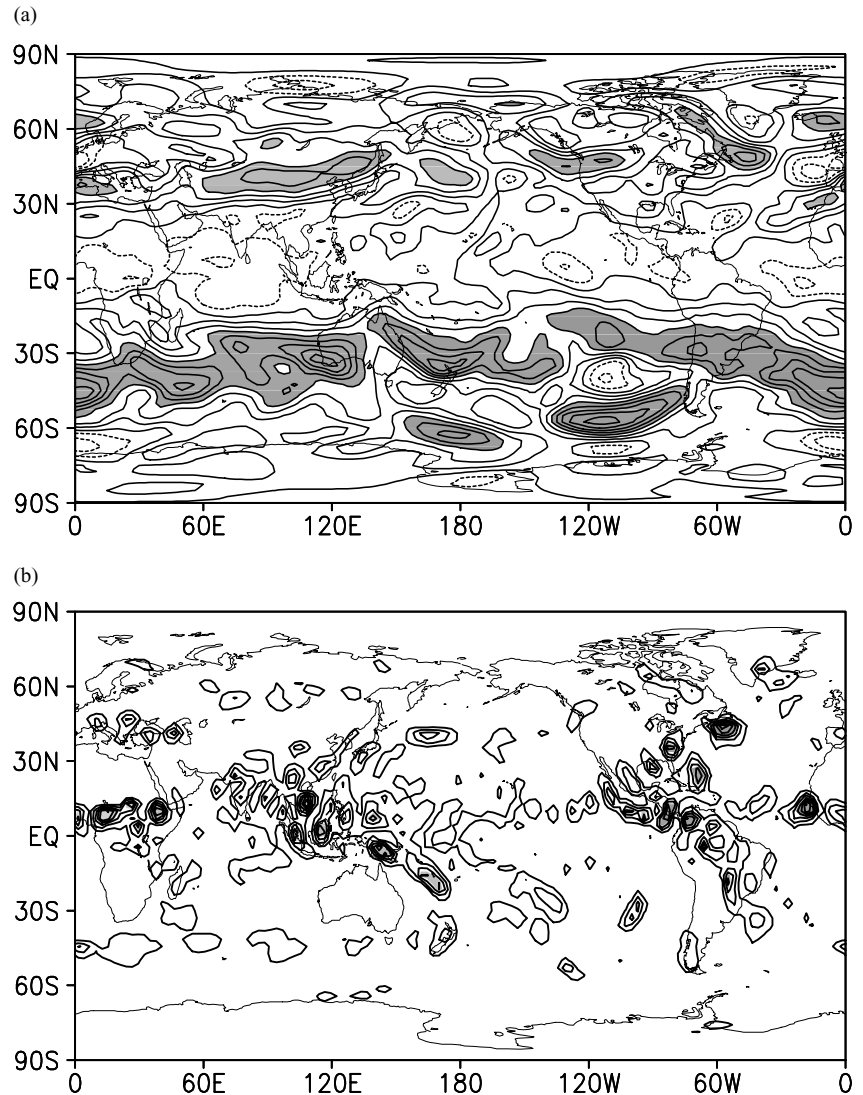

Fig 1. (a) Zonal wind analysis at 300 hPa and valid at 00 UTC 3 September 1996. The contour interval is 10.0 m, and negative values are dashed and values larger than 30.0 m shaded. (b) Accumulated precipitation of the forecast over 36 h. The contour interval is 10.0 mm, and values larger than 30.0 mm are shaded.

3. Singular vectors without filtering

We examine the characteristics of SVs without filtering to establish the reference for the effect of filtering. The projection operator confines the domain of computation of the energy norm (2) to the Northern Hemisphere. The optimization time interval is taken as 36 h. We analyze the leading 10 SVs, as their singular values decrease relatively quickly in comparison with the later singular values when the time window is 24 h (as also observed by Buizza, 1994).

In the linearized model, the basic state is a model forecast, which starts from the initialized analysis valid at 00 UTC 3 September 1996, using the full-physics model. Fig. 1 shows the zonal wind component of the initial condition at 300 hPa and the

36-h accumulated precipitation of the forecast. The perturbation of the basic state, which constitutes leading SVs is mostly located on the southern flank of the jets and their exit areas (not shown in the figure) as pointed by Buizza and Palmer (1995) and Hoskins et al. (2000).

3.1. Model without physics

In the present context, the model without physics comprises the dynamic core with simple horizontal diffusion and surface drag (case NP). For this model, we find that seven of the 10 leading SVs are dominated by the spurious modes, which are characterized by the vertical and horizontal perturbations with two-grid size wavelength. As an example, Fig. 2 presents the horizontal
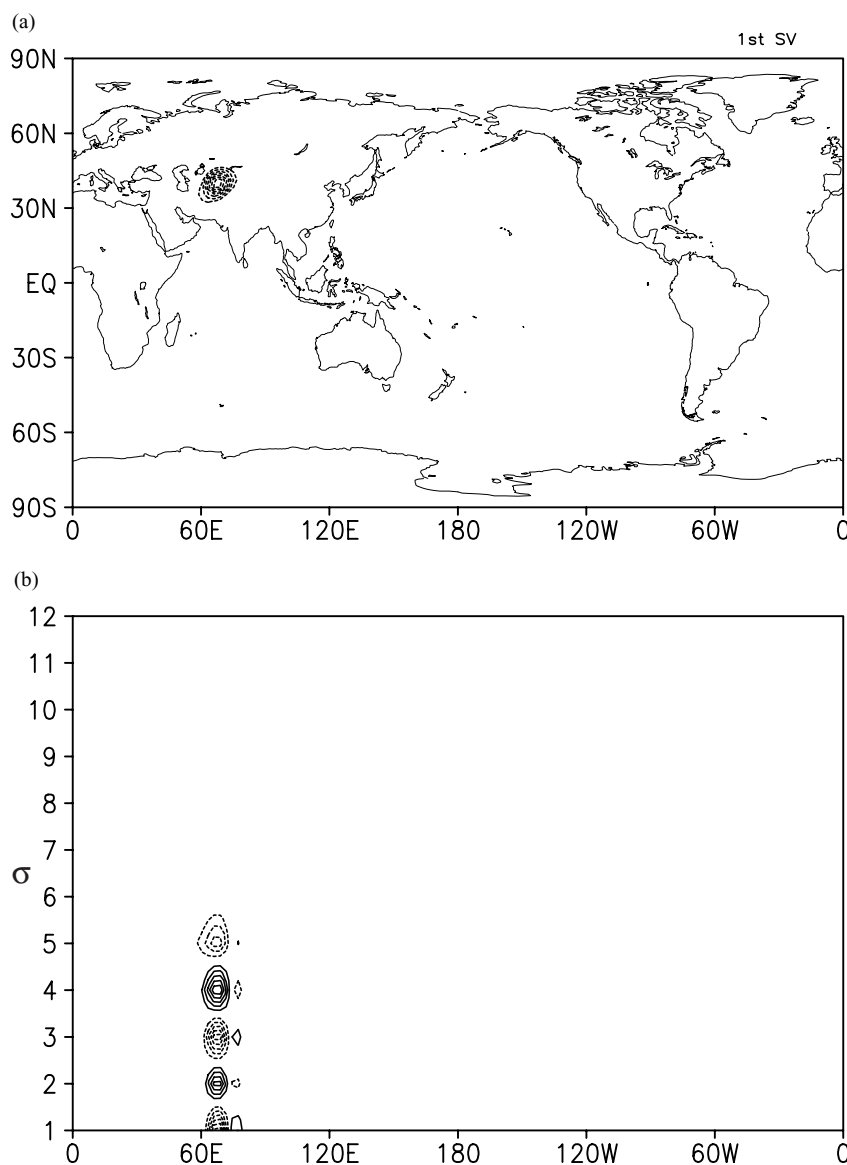

Fig 2. The first SV of the case where only simple horizontal diffusion and the surface drag are included in the model physics and with an optimal time interval of 36 h. (a) The streamfunction at 800 hPa, and (b) the longitude-model level cross-section of temperature at 40°N. This SV is representative of the structure of spurious modes.
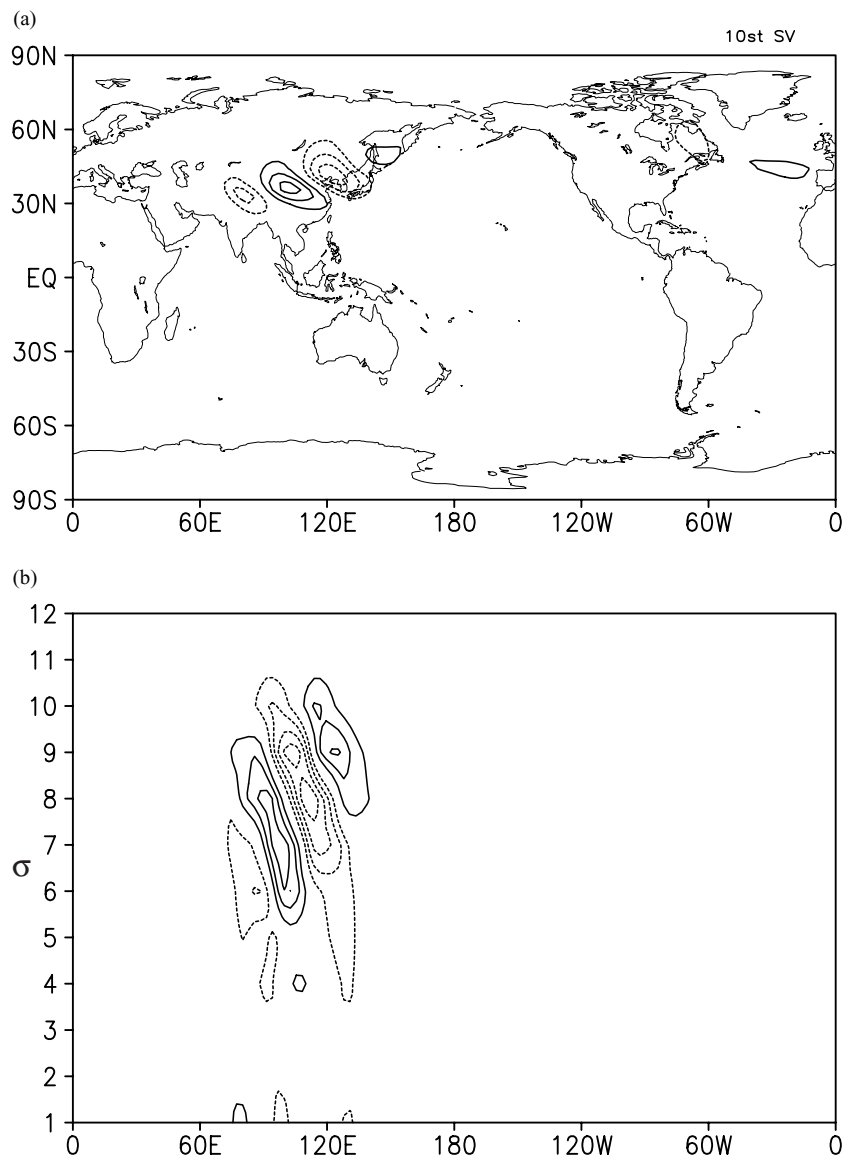
(a)

10st SV

(b)

Fig 3. Same as Fig. 2, but for the tenth SV. (a) The streamfunction at 500 hPa, and (b)the longitude-model level cross-section of temperature at 45°N.

structures at 800 hPa and the vertical-height section structure of the first SVs. Such structures have also been identified in the ECMWF model by Buizza (1994). The three-point spatial scale of the spurious modes suggests the possibility of suppressing them by spatial filtering discussed in the next section.

The three SVs that appear to be 'meteorological' in the sense of Buizza et al. (1993) are the seventh, ninth, and tenth. For instance, the horizontal and vertical structures of the tenth SV are plotted in Fig. 3, which shows its major perturbations are located in the southern flank of the Asia Jet. Zeng (1983) argues that the perturbation extracts barotropic energy from the basic jet stream as seen in the horizontal structure in (Fig. 1). Hoskins et al. (2000) and Barcilon and Bishop (1998) explain that the vertical structure is a typical mid-latitude baroclinically growing non-normal mode. In the following, we identify the 'meteorological'

modes by visually examining their vertical and horizontal structures and only those showing horizontal connected structures and vertical perturbations deeper than four vertical model levels are considered as reasonable modes.

3.2. Model with the boundary-layer physics

We first include the boundary-layer physics and vertical diffusion in the model (case BP). In order to compare the SVs from cases NP and BP, we follow Buizza et al. (1993) and Buizza (1994) and compute the so-called projection matrix:

$$m_{ij}(\text{NP, BP}) = [\langle v_i(\text{NP}); E v_j(\text{BP})\rangle]^2.$$

Each element of the projection matrix is the squared scalar product of the ith SV of case NP and the jth SV of case BP. As

Table 1. The projection matrix for cases NP and BP. The indices on the first row refer to case NP, and the indices on the first column to case BP. Each entry m_{ij} of the matrix gives the square scalar product between the ith SV of case NP and the jth SV of case BP; that is, the percentage of energy of the ith SV of case NP explained by the jth SV of case BP. The last row gives the percentages of energy of the ith SV of case NP by all 10 SVs of case BP

	1	2	3	4	5	6	7	8	9	10
1	78	0	0	0	19	0	0	0	0	0
2	0	0	0	0	0	0	0	0	0	0
3	0	0	36	0	0	33	0	15	0	0
4	0	0	0	0	0	0	81	0	0	0
5	0	0	0	0	0	0	4	0	0	0
6	0	0	27	0	0	49	0	4	0	0
7	0	0	0	0	0	0	0	0	89	3
8	0	0	0	0	0	0	0	0	4	85
9	6	0	0	0	38	0	0	0	0	1
10	0	0	0	0	0	0	0	0	0	4
	85	0	64	0	58	84	85	20	94	94

such, it represents the amount of energy of the ith SV of the NP case that is explained by the jth SV of the BP case. The sum of the matrix elements with a fixed index represents how well the ith SV of the NP case can be reconstructed from a linear combination of the first N SVs of the BP case.

A measure of similarity based on projection of a set of SVs on another is provided by the similarity index of the two cases NP and BP and is defined as

$$s(A, B; N) = \frac{1}{N} \sum_{i,j=1}^{N} m_{i,j}(A, B)$$

(which measures the similarity between the unstable subspaces spanned by the first N SVs of each case). The index equals unity if the unstable subspaces of the two cases are identical.

The projection matrix (Table 1) shows that the seventh SV of case NP resembles the fourth SV of case BP, the ninth SV of case NP resembles the seventh SV of case BP, and the tenth SV of case NP resembles the eighth SV of case BP. These three SVs are the 'meteorological' ones in the sense of Buizza et al. (1993) for case NP. In case BP, the tenth SV is also 'meteorological' in the same sense. We observe that the incorporation of the boundary-layer physics and the vertical diffusion leads to limited improvement in the structure of the SVs; while the three SVs from the case with no physics persist in the present case, an additional reasonable SV (tenth SV) appears, but there are still six SVs that are spurious. Our observation is similar to that of Buizza (1994).

3.3. Model with the full physics

In the following, we incorporate all the physical processes in the non-linear model, as described in Section 2.1, into the adjoint

model (case FP) and show that it leads to a substantial improvement of SVs.

Figure 4 presents the vertical and horizontal structures of the sixth SV, which may be viewed as representative of the three SVs consisting of tropical modes. The major perturbations are geographically co-located with the major tropical precipitation areas. In the vertical direction, the structure of the sixth SV is localized mainly in the upper model and middle-lower model levels. The upper part is characterized by a slight tilt toward the east and is understood to be associated with an easterly baroclinic structure. The middle-lower level part is generally understood to have a barotropic structure. Such structure features distinguish these tropical modes from the spurious barotropic and inertial unstable modes that have been comprehensively analyzed by Barkmeijer et al. (2001). However, these three SVs are contaminated to some degree by inertial unstable modes, as indicated by the perturbation centers located between 200 and 300 hPa.

As expected, all three reasonable SVs obtained for both the NP and BP cases are the leading SVs for case FP. This is evidenced by the values of projection matrix entries amongst the three cases being larger than 80% in the projection matrix (not shown). The new leading SVs include the tropical modes discussed above and also new leading SVs, which are mainly located over the Atlantic Ocean as shown in Fig. 5.

Thus, the full-physics model is found to suppress rather effectively the spurious modes, which may possibly be a common feature of all GCMs with full physics. This is due to (i) the surface energy flux, boundary-layer physics, and vertical diffusion being treated in a consistent manner, and (ii) some physical processes, such as the dry convective adjustment and radiative transfer, playing an energy diffusion role.

We observe that the full-physics model brings forth the tropical modes among the leading SVs. Then a natural question arises as to the impact of the full-physics model on the SVs that are mainly located at mid-latitudes and higher latitudes. In order to answer this question, we compute these SVs while the projection operator is defined over the area north of 30° N.

Then the projection matrix, as defined before, is computed for comparing the cases for 30°N and the Northern Hemisphere. The three SVs consisting of tropical modes (i.e. the second, third and sixth SVs of case FP) are not present in the case for 30°N, as indicated by the zero value of the indices (Table 3). There are three SVs (i.e. the fourth, fifth, and tenth) of case FP that are present in the case for 30°N. These three SVs are also obtained in cases NP and BP. Thus, these three SVs are not affected by the physical processes.

Now we analyze the effect of the inclusion of the full physics on the singular values (Table 2). The three SVs located in mid-latitudes present in all three cases of case NP, case BP, and case FP, respectively, have close singular values. This implies that the model physical processes have little impact on the singular values of these SVs.
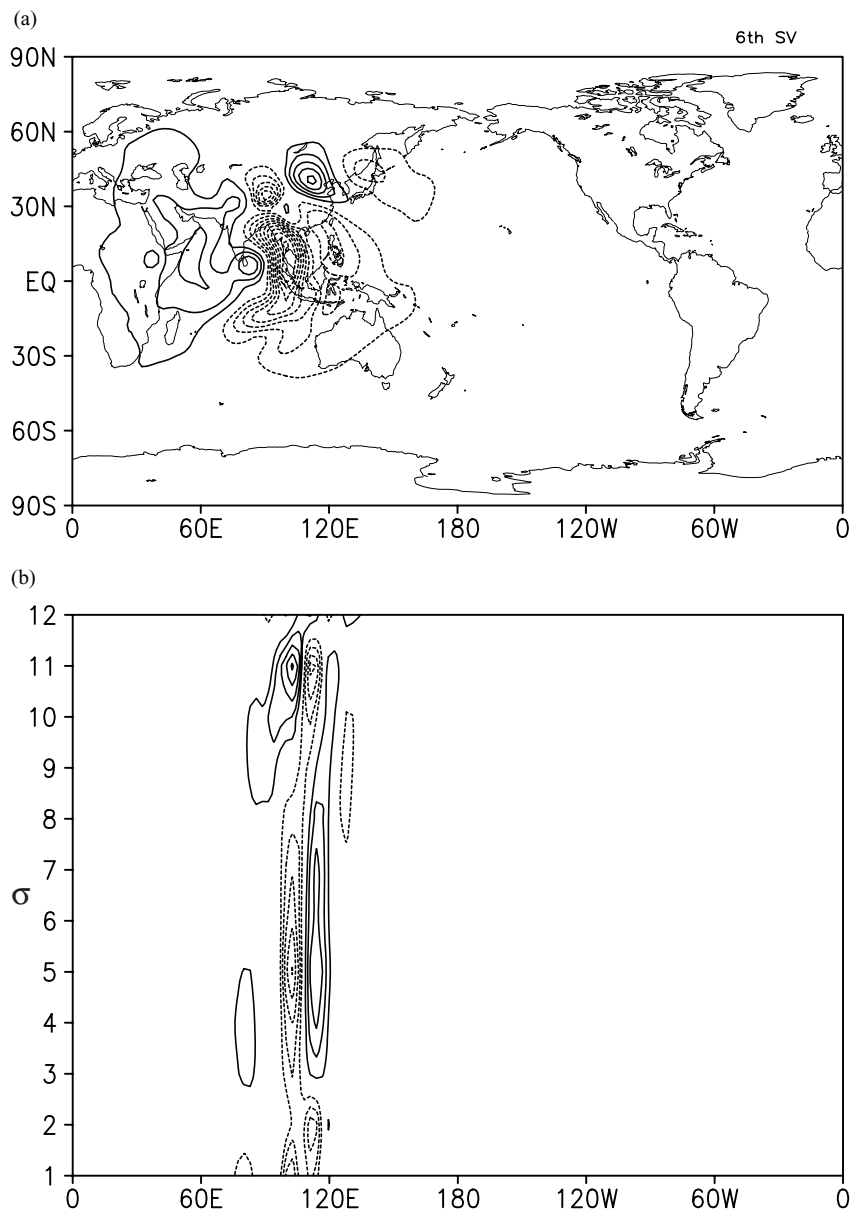
(a)

(b)

Fig 4. The sixth SV of the case where the full physics is included in the linearizations and with an optimal time interval of 36 h. (a) The streamfunction at 500 hPa, and (b) the longitude-model level cross-section of temperature at 1°N.

In contrast, precipitation significantly increases the growth rate of the SVs when their modes are located in the tropics. Here we do not suggest that there are new modes excited solely by precipitation, since these modes are evidently baroclinic. The combination of the baroclinity and precipitation latent heating leads those modes to larger singular values and then they become leading SVs. The conclusion here is that the precipitation enhances growth rates of SVs only when they geographically overlap with precipitation areas.

These results concur with results obtained by Errico et al. (2001) pointing out that the primary effect of considering moist physics in the model leads to faster growth of perturbations than in the dry situation (see also Ehrendorfer et al., 1999). The impor-

tant point made by Errico and Ehrendorfer is that moist physics in the linear models enables new instability mechanisms to be triggered, leading to new SV structures. This can be seen from the first singular value for all the three cases (Table 2).

4. Dynamically filtered singular vectors for the full-physics model

The inclusion of the full physics has substantially improved the computation of SVs as it has to a great degree suppressed the spurious modes and also enhanced the growth of the modes present in the leading SVs. However, there still exist some deficiencies. For instance, spurious modes have not been completely
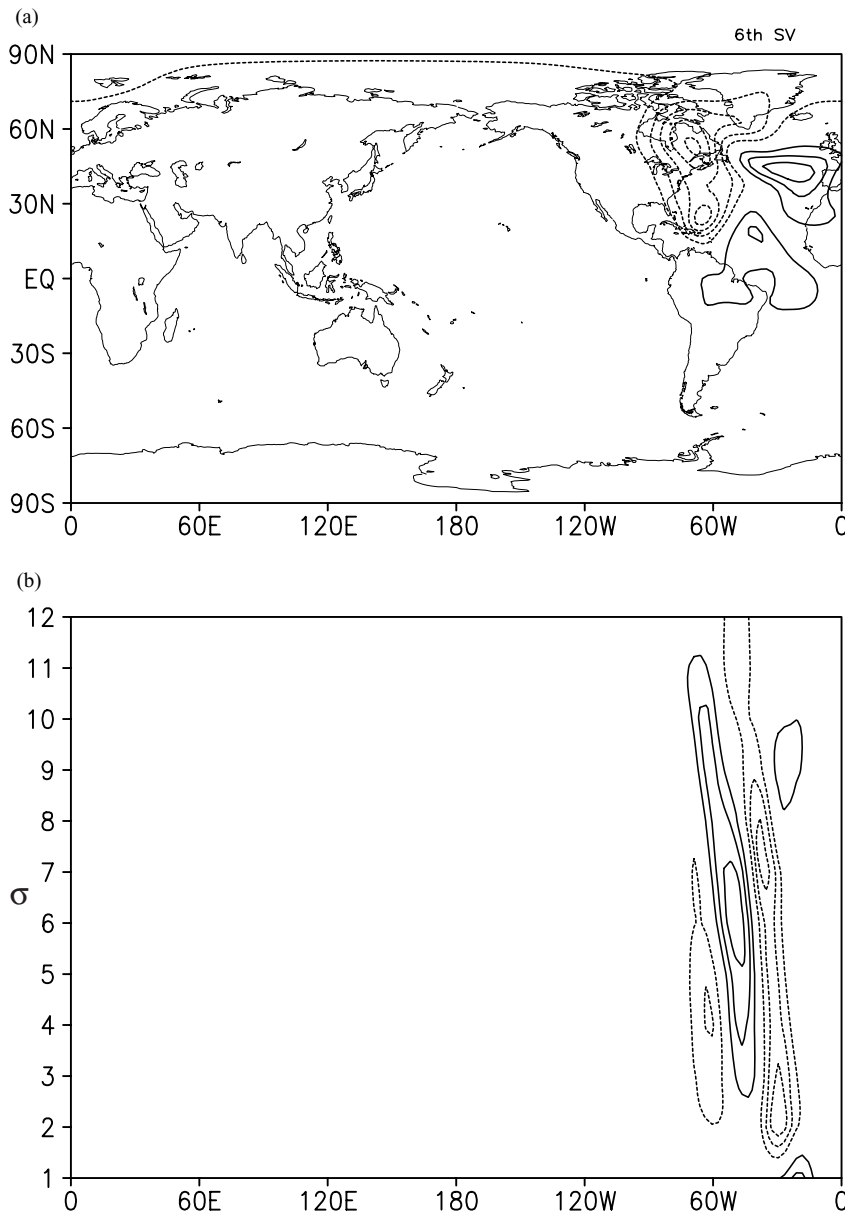
(a)

(b)

Fig 5. Same as in Fig. 4, but for the eighth SV. (a) The streamfunction at 500 hPa, and (b) the longitude-model level cross-section of temperature at 50°N.

eliminated in the leading SVs, and SVs in Fig. 3a have horizontal spatial scales of only a few hundred kilometers, which is smaller than typical synoptic scales.

The present filtering method involves the dynamics of the model and controls the computation of SVs. These filtering operators include both spatial and temporal filters, as well as the rotational projection used by Errico (2000a).

The spatial filter can be applied to the initial condition, which then is equivalent to an initialization process. It can also be applied at the final time of the time window. The results are found to be insensitive to the filtering at the end of the time window. For example, F_t in eq. (8) is a truncation operation that truncates the field at T15, and we find no measurable difference in the computed leading SVs.

Spurious modes are well suppressed in the computed leading SVs when we use the model with full physics and apply the spatial truncation at resolution T21 to the initial condition, as well as implement the projection of the wind fields on to the rotational projector (Errico, 2000a). Figure 9 presents the first 10 square singular values for the leading 10 SVs for the optimization time window of 24 h. Those spurious modes with isolated small spatial scale perturbations do not exist in all 10 leading SVs.

Let us further examine how the filtering affects the meteorological modes significantly. By examining the singular values, we have seen that those SVs consisting of the meteorological modes show the values to be reduced by about 50% (Table 4). As expected, their structure has larger scales. The combined perturbations of all 10 SVs appear to cover the extratropics, which

Table 2. The singular values for cases NP, BP, and FP. The three singular values with the superscript *a* denote that their associated SVs have similar structures, and the same meaning holds for *b* and *c*

Cases	Case NP	Case BP	Case FP
λ_1^2	277	123	9569
λ_2^2	208	38	32
λ_3^2	100	28	**25**[a]
λ_4^2	75	**25**[a]	**22**[b]
λ_5^2	55	24	**21**[c]
λ_6^2	43	23	20
λ_7^2	**29**[a]	**23**[b]	17
λ_8^2	28	**21**[c]	17
λ_9^2	**23**[b]	20	16
λ_{10}^2	**22**[c]	17	15

Table 3. The projection matrix for two FP cases of spatial projection operators for 30°N latitude and the Northern Hemisphere. The indices on the first row refer to the case where the spatial projecting operator is defined to include area north of 30°, while the indices on the first column to the case where the spatial projecting operator excludes the Southern Hemisphere. Each entry m_{ij} of the matrix gives the square scalar product between the *i*th SV of the 30° case and the *j*th SV of the Northern Hemisphere case; that is, the percentage of energy of the *i*th SV of the 30° case explained by the *j*th SV of the Northern Hemisphere case. The last row provides the percentages of energy of the *i*th SV of the 30° case by all 10 SVs of the Northern Hemisphere case

	1	2	3	4	5	6	7	8	9	10
1	99	0	0	0	0	0	0	0	0	0
2	0	0	0	98	0	0	0	0	0	0
3	0	0	0	0	97	1	0	0	0	0
4	0	0	0	0	0	0	73	11	13	0
5	0	0	0	0	0	0	0	0	0	87
6	0	0	0	0	0	0	0	1	0	0
7	0	0	0	0	0	0	0	0	0	2
8	0	0	0	0	0	0	0	0	0	0
9	0	0	0	0	0	0	0	0	0	0
10	0	0	0	0	0	0	0	0	0	0
	99	0	0	99	97	2	74	12	14	92

Fig 6. The first three SVs of the case where the full physics is included in the linearizations and over an optimization time interval of 24 h.

is desired by ensemble forecasts. It is interesting to note that all the reasonable meteorological SVs at middle latitudes in case NP have comparable ones (in terms of both the geographical location and spatial structure) as indicated typically by the first, fourth and ninth SVs. Those modes excited by physics in the tropics and subtropics in case FP also have comparable ones, but only in terms of the geographical location. The tropical perturbation with filtering presents well-organized wave train structure as indicated by the eighth SV, which may be attributed to the use of only the rotational wind (see Errico, 2000a,b).
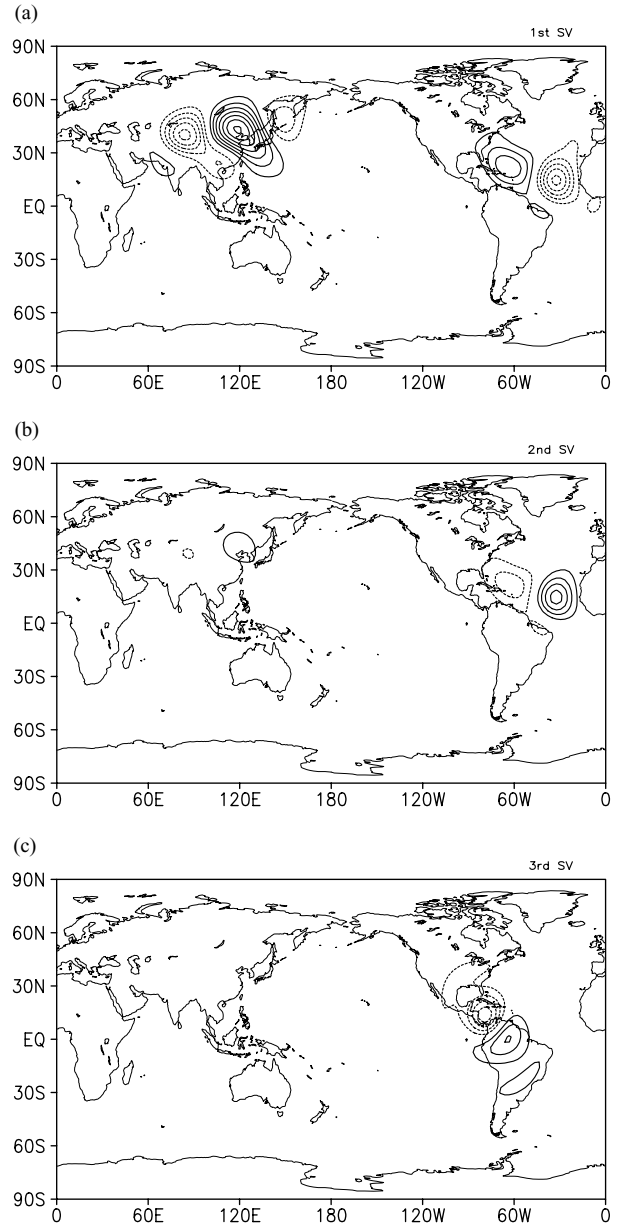
As the computation of SVs is based on a linearized model, the role of filter in this situation is similar to that of turbulence, which is equivalent in a sense to diffusion that exerts stronger effect on perturbations of smaller scales than of larger scales.

When the time filter is applied, eq. (6) is generalized as

$$\lambda^2 = \frac{\int_s^t \langle Px_\tau, E_\tau Px_\tau \rangle \, d\tau}{(t-s)\langle x_0, E_0 x_0 \rangle}. \tag{9}$$

Here, we take $t - s$ to be 6 h, while the optimization time interval is 36 h. The results indicate that such a filter relatively enhances spuriously growing modes. All 10 SVs consist of
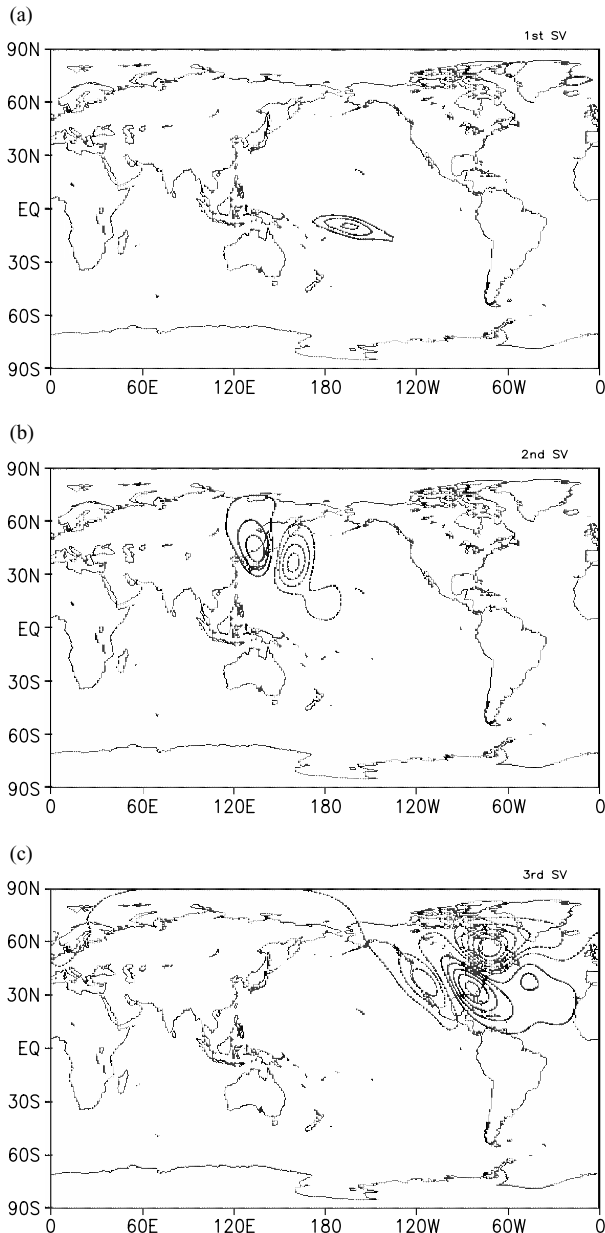
(a)

(b)

(c)

Fig 7. Same as Fig. 6, but for 12 UTC 24 June 1994.

(a)

(b)

(c)

Fig 8. Same as Fig. 7, but for the case without moisture (NM).

non-meteorological modes for case NP. Since the spuriously growing modes are locally standing perturbations, they are not weakened by the time filtering. On the other hand, the meteorological modes which consist of traveling perturbations are weakened by the time filter.

5. Re-examination of moisture processes

The above discussion concerns the case where the basic state of the model forecast is obtained from an initialized analysis valid at 00 UTC 3 September 1996. A careful examination of Fig. 1 shows that the precipitation over the Northern Hemisphere is relatively
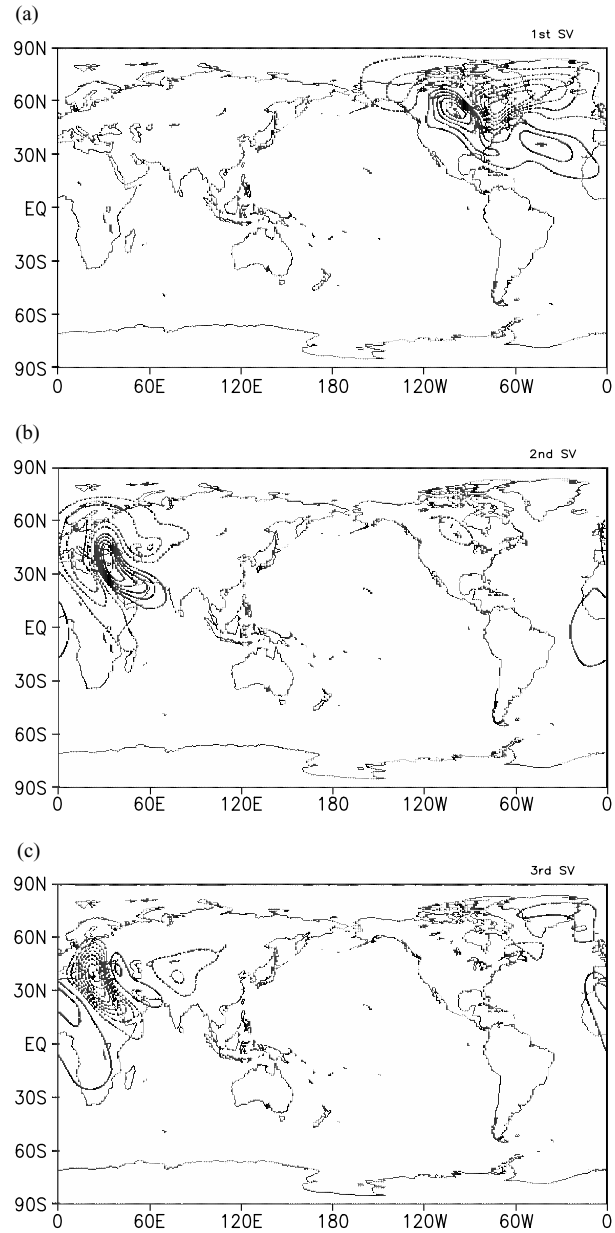
weak, and is mostly located in the tropical area. We consider a new case (precipitation case) in which the linearization is carried out around the basic state of the model forecast obtained from the initialized analysis valid at 12 UTC 24 June 1994 when the Indian monsoon was active. The precipitation is stronger and it covers more extensive areas than in the first case. SVs are computed with filter, that is, the truncation at resolution T21 is applied to the initial condition, along with projecting the wind fields on to the rotational components (Errico, 2000a). Figure 7 displays the first three leading SVs for the precipitation case. Figure 8 is the same as Fig. 7, but for the case without moisture (NM).
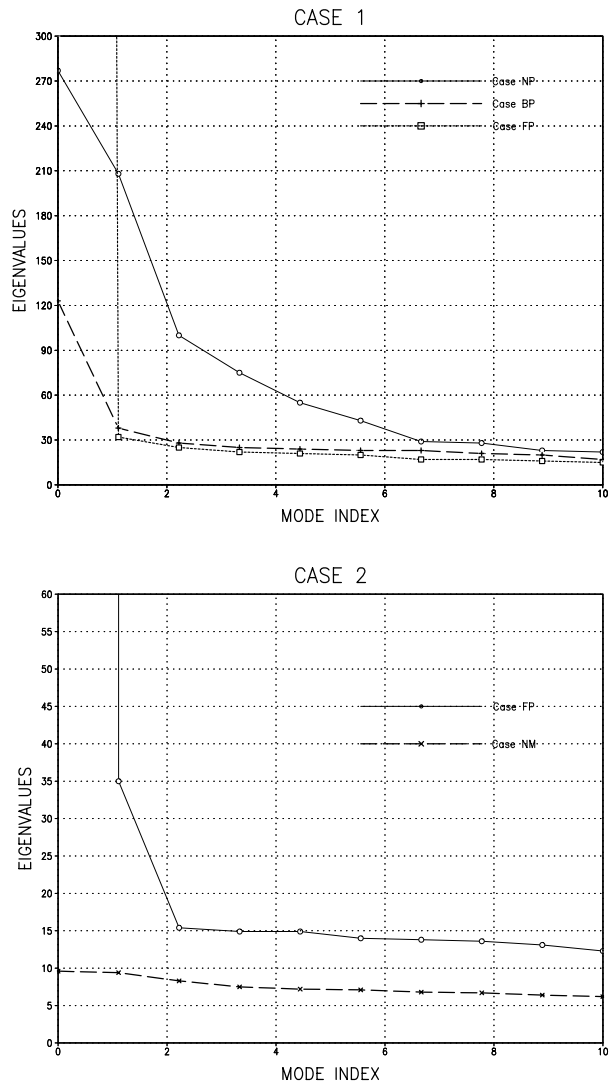
Fig 9. Squared singular values for the leading 10 SVs compared (a) using full physics (FP), boundary layer physics (BP) and no physics (NP) versions for the first test case and (b) for the second 12 UTC 24 June 1994 case for full physics (FP) and no moisture (NM).

Table 4. The singular values for cases FP and NM in the experiments with strong precipitation for the case at 12 UTC 24 June 1994

Cases	Case FP	Case NM
λ_1^2	4.9×10^6	9.6
λ_2^2	35.0	9.4
λ_3^2	15.4	8.3
λ_4^2	14.9	7.5
λ_5^2	14.9	7.2
λ_6^2	14.0	7.1
λ_7^2	13.8	6.8
λ_8^2	13.6	6.7
λ_9^2	13.1	6.4
λ_{10}^2	12.3	6.2

Table 5. Singular values for case FP (full physics) with and without filtering for a time window of 24 h for test case 00 UTC 3 September 1996

Cases	Case with filtering	Case without filtering
λ_1^2	410	1932
λ_2^2	6.59	21.0
λ_3^2	6.52	19.8
λ_4^2	6.03	17.1
λ_5^2	5.88	14.3
λ_6^2	5.45	13.2
λ_7^2	5.32	12.5
λ_8^2	4.95	10.9
λ_9^2	4.82	10.5
λ_{10}^2	4.60	8.60

This case confirms the conclusion about the effect of precipitation on SVs from the previous case. To single out the effect of precipitation, we further perform two experiments. One experiment uses the full physics, and the other turns off the moisture processes. The precipitation excites new SVs as in the previous case. The eighth SV in Fig. 7 is the precipitation excited new SV, since it disappears when the moisture process is turned off (not shown). In Fig. 7, four SVs (i.e. the fifth, sixth, eighth, and tenth) have perturbations well overlapping with the monsoon precipitation areas, while the other two SVs (the second and third) overlap with other precipitation areas (not shown). These six SVs have a comparable counterpart in the case without moisture process. We see that the moisture process leads to a shift of the perturba-

tions of the six SVs toward the equator, and their singular values are 30–50% larger than those without the moisture process (Table 5). In contrast, the seventh SV also has a comparable counterpart in the case without the moisture process, and they have close singular values. These results are consistent with the conclusion that the precipitation enhances growth rates of SVs only when their perturbations geographically overlap with precipitation areas.

It should be pointed out that the first SV consists of spurious modes in this case. Its singular value is as large as 4.9×10^6. As this SV disappears when the moisture process is turned off, it may be attributed to the singularities inherent in modeling the moisture process, which has been well documented and described by Errico and Raeder (1999). The presence of this SV may point to the fact that applying wave truncation and dynamical balance restriction to the initial values is not able to remove spurious modes due to the discontinuities in the adjoint model when strong precipitation occurs.

6. Summary of results and conclusions

The present results are consistent with the observations of Ehrendorfer et al. (1999) and Barkmeijer et al. (2001) on the impact of physical processes on SVs. The impact of physics on SVs can be substantial in a global model even for an optimization time interval as short as 24 h. The growth rates are significantly enhanced and the structures are significantly altered by the inclusion of physics. However, we have noticed that physical processes, especially precipitation, affect a leading SV fundamentally only when the SV perturbation is geographically coupled with precipitation. For those SVs that are geographically independent of precipitation, physics has little impact on either their growth rate or the structure. The impact of physics is characterized by localization. Actually, in our case, physics exerts little impact on the structure of the computed SVs when the projection operator is confined to 30° N. This is simply due to the fact that precipitation occurs mainly in the tropics and subtropics and cannot overlap with SV perturbations.

The FSUGSM model appears to have more leading SVs dominated by spurious modes than the ECMWF model (Buizza, 1994). A possible reason may be that this version of the FSUGSM has a relatively low vertical resolution. Specifically, this version of the FSUGSM has only 12 levels in the vertical direction, while ECMWF models have at least 19 levels.

Another reason is related to the scheme of moisture parametrization used in our experiments, i.e. the modified Kuo (1974) scheme instead of the relaxed Arakawa and Schubert (1974) scheme. Research work by DeWitt (1996) has shown that integrations performed with the relaxed Arakawa–Schubert scheme better approximate the precipitation gradients in the tropics than when the Kuo scheme is used. We note that the spatial filter coupled with the operator that projects the flow winds to the rotational wind improves the structural features of the computed SVs and is beneficial in the suppression of spuriously growing modes. On the other hand, the temporal filter seems to enhance spurious modes as discussed in Section 4.

The spatial filter plays a role similar to an initialization process in numerical weather prediction. Theoretically, an operational initialization procedure could be more reasonable and also feasible to implement. However, the computational cost of carrying out an operational initialization procedure during the computation of the SVs is prohibitively expensive. As evidenced by this study, a simple filtering procedure could play the role of an initialization procedure to some degree. When spatial filtering and some flow balance constraints are appropriately combined, we can expect a satisfactory filtering procedure for the computation of SVs. Further, this procedure can always be used to control the structure of SVs for mitigating the effect of linearization.

Note that the filtering process does not appear to affect the physical processes. However, it should be carefully verified in each instance, since geographical locations and growth rates of spurious modes are very sensitive to background flows and model physics. If one cannot guarantee that the SVs are free of spurious modes, one risks drawing incorrect conclusions on the effect of physical processes due to the interference of spurious modes.

This paper raises two research issues worth investigating. The first is to verify the effectiveness and the benefit of the filtering technique in an operational setting such as an ensemble forecast. The second issue is to investigate if the filtering technique still plays a useful role when the error covariance is introduced, as discussed by Barkmeijer et al. (1998, 1999). Technically, the filtering process proposed in this paper can still be implemented in such a case, but its usefulness may depend on the characteristics of the error covariance matrix.

The effect of moisture on the number of growing structures as well as the specification of appropriate norms to properly account for moist processes are issues that remain to be studied.

7. Acknowledgments

References

Arakawa, A. and Schubert, W. H. 1974. Interaction of a cumulus ensemble with the large-scale environment. Part I. *J. Atmos. Sci.* **31**, 674–704.

Barcilon, A. and Bishop, C. 1998. Non-modal development of baroclinic waves undergoing horizontal shear deformation. *J. Atmos. Sci.* **55**, 3583–3597.

Barkmeijer, J. 1992. Local error growth in a barotropic model. *Tellus* **44A**, 314–323.

Barkmeijer, J., van Gijzen, M. and Bouttier, F. 1998. Singular vectors and estimates of the analysis error covariance matrix. *Q. J. R. Meteorol. Soc.* **124**, 1695–1713.

Barkmeijer, J., Buizza, R. and Palmer, T. N. 1999. 3D-Var Hessian singular vectors and their potential use in the ECMWF ensemble prediction system. *Q. J. R. Meteorol. Soc.* **125**, 2333–2351.

Barkmeijer, J., Buizza, R., Palmer, T. N., Puri, K. and Mahfouf, J.-F. 2001. Tropical singular vectors computed with linearized diabatic physics. *Q. J. R. Meteorol. Soc.* **127**, 685–708.

Borges, M. D. and Hartmann, D. L. 1992. Barotropic instability and optimal perturbations of observed non-zonal flow. *J. Atmos. Sci.* **49**, 335–354.

Businger, J. A., Wyngard, J. C., Izumi, Y. and Bradley, E. F. 1971. Flux profile relationships in the atmospheric surface layer. *J. Atmos. Sci.* **28**, 181–189.

Buizza, R. 1994. Sensitivity of optimal unstable structures. *Q. J. R. Meteorol. Soc.* **120**, 429–451.

Buizza, R. and Montani, A. 1999. Targeting observations using singular vectors. *J. Atmos. Sci.* **56**, 2965–2985.

Buizza, R. and Palmer, T. N. 1995. The singular vector structure of the global atmospheric global circulation. *J. Atmos. Sci.* **52**, 1434–1456.

Buizza, R., Tribbia, J., Molteni, F. and Palmer, T. N. 1993. Computation of optimal unstable structures for a numerical weather prediction model. *Tellus* **45A**, 388–407.

Buizza, R., Gelaro, R., Molteni, F. and Palmer, T. N. 1997. The impact of increased resolution on predictability studies with singular vectors. *Q. J. R. Meteorol. Soc.* **123**, 1007–1033.

Coutinho, M. M., Hoskins, B. J. and Buizza, R. 2004. The influence of physical processes on extratropical singular vectors. *J. Atmos. Sci.* **61**, 195–209.

de Pondeca, M. S. F. V., Barcilon, A. and Zou, X. 1998. An adjoint sensitivity study of the efficacy of modal and non-modal perturbation in causing model block onset. *J. Atmos. Sci.* **55**, 2095–2118.

DeWitt, D. 1996. The Effect of the Cumulus Convection on the Climate of the COLA General Circulation Model. COLA Technical Report No. 27, Center for Ocean–Land–Atmosphere Studies, Calverton, MD 20705, USA.

Ehrendorfer, M. and Tribbia, J. J. 1997. Optimal prediction of forecast error covariance through singular vectors. *J. Atmos. Sci.* **54**, 286–313.

Ehrendorfer, M., Errico, R. M. and Raeder, K. D. 1999. Singular vector perturbation growth in a primitive equation model with moist physics. *J. Atmos. Sci.* **56**, 1627–1648.

Errico, R. M. 2000a. Interpretations of the total energy and rotational energy norms applied to determination of singular vectors. *Q. J. R. Meteorol. Soc.* **126**, 1581–1599.

Errico, R. M. 2000b. The dynamical balance of leading singular vectors in a primitive-equation model. *Q. J. R. Meteorol. Soc.* **126**, 1601–1618.

Errico, R. M. and Raeder, K. D. 1999. An examination of the accuracy of the linearization of a mesoscale model with moist physics. *Q. J. R. Meteorol. Soc.* **125**, 169–195.

Errico, R. M., Ehrendorfer, M. and Raeder, K. D. 2001. The spectra of singular values in a regional model. *Tellus* **53A**, 317–332.

Farrell, B. F. 1988. Optimal excitation of neutral Rossby waves. *J. Atmos. Sci.* **45**, 163–172.

Farrell, B. F. 1989. Optimal excitation of baroclinic wave. *J. Atmos. Sci.* **46**, 1193–1206.

Gelaro, R., Buizza, R., Palmer, T. N. and Klinker, E. 1998. Sensitivity analysis of forecast errors and the construction of optimal perturbations using singular vectors. *J. Atmos. Sci.* **55** 1012–1037.

Haltiner, G. J. and Williams, R. T. 1980. *Numerical Prediction and Dynamic Meteorology*, 2nd edition. Wiley, New York, 477 pp.

Hansen, J. A. and Smith, L. A. 2000. The role of operational constraints in selecting supplementary observations. *J. Atmos. Sci.* **57** 2859–2871.

Harshvardan, R. and Corsetti, T. G. 1984. Long-wave parametrization for the UCLA/GLAS GCM. NASA Technical Memo. 86072, Goddard Space Flight Center, Greenbelt, MD 20771, 52 pp.

Hartmann, D. L., Buizza, R. and Palmer, T. N. 1995. Singular vectors: the effect of spatial scale on linear growth of disturbances. *J. Atmos. Sci.* **52**, 3885–3894.

Hoskins, B. J., Buizza, R. and Badger, J. 2000. The nature of singular vector growth and structure. *Q. J. R. Meteorol. Soc.* **126**, 1565–1580.

Kanamitsu, M., Tada, K., Kudo, K., Sato, N. and Isa, S. 1983. Description of the JMA operational spectral model. *J. Meteorol. Soc. Japan* **61**, 812–828.

Krishnamurti, T. N., Xue, J., Bedi, H. S., Ingles, K. and Oosterhof, D. 1991. Physical initialization for numerical weather prediction over the tropics. *Tellus* **43A**, 53–81.

Krishnamurti, T. N., Bedi, H. S. and Ingles, K. 1993. Physical initialization using the SSM/I rain rates. *Tellus* **45A**, 247–269.

Kuo, H-L. 1974. Further studies of the parametrization of the influence of cumulus convection on large-scale flow. *J. Atmos. Sci.* **31**, 1232–1240.

Lacis, A. A. and Hansen, J. E. 1974. A parametrization of the absorption of solar radiation in the Earth's atmosphere. *J. Atmos. Sci.* **31**, 118–133.

Lehoucq, R. B., Sorensen, D. C. and Yang, C. 1998. ARPACK *Users' Guide: Solution of Large-scale Eigenvalue Problems with Implicitly Restarted Arnoldi Methods*, Software, Environments, and Tools Series, Vol. 6, SIAM, Philadelphia, 160 pp.

Li, Z. and Ji, L. 1996. Internal dynamics of the generation of atmospheric teleconnection patterns. *Adv. Atmos. Sci.* **13**, 19–32.

Li, Z. and Ji, L. 1997. Efficient forcing and teleconnection patterns. *Q. J. R. Meteorol. Soc.* **123**, 2401–2423.

Li, Z., Navon, I. M. and Zhu Y. 2000. Performance of 4D-Var with different strategies on the use of adjoint physics with the FSU Global Spectral Model. *Mon. Wea. Rev.* **128**, 668–688.

Liu, Z. and Navon, I. M. 2002. Documentation of the Tangent Linear and Adjoint Models of New MPI Version of the FSU Global Spectral Model. Technical Report, 39 pp (available from http://www.csit.fsu.edu/~navon/pubs/).

Lorenz, E. N. 1965. A study of the predictability of a 28 variable atmospheric model. *Tellus* **17**, 321–333.

Lorenz, E. N. and Emanuel, K. A. 1998. Optimal sites for supplementary observations: simulation with a small model. *J. Atmos. Sci.* **55**, 399–414.

Louis, J.-F. 1979. A parametric model of vertical eddy fluxes in the atmosphere. *Boundary Layer Meteorology* **17**, 187–202.

Mahfouf, J.-F. 1999. Influence of physical processes on the tangent-linear approximation. *Tellus* **51A**, 147–166.

Mahfouf, J.-F., Buizza, R. and Errico, R. M. 1996. Strategy for including physical processes in the ECMWF variational data assimilation system. In: *Proceedings of the 1996 ECMWF Seminar on Data Assimilation and Workshop on Non-Linear Aspects of Data Assimilation*, ECMWF, 595–632, (available from ECMWF, Shinfield Park, Reading, Berkshire RG2 9AX, UK).

Molteni, F. and Palmer, T. N. 1993. Predictability and finite-time instability of the northern winter circulation. *Q. J. R. Meteorol. Soc.* **119**, 269–298.

Molteni, F., Buizza, R., Palmer, T. N. and Petroliagis, T. 1996. The new ECMWF ensemble prediction system: methodology and validation. *Q. J. R. Meteorol. Soc.* **122**, 73–119.

Montani, A. and Thorpe, A. J. 2002. Mechanisms leading to singular vector growth for FASTEX cyclones. *Q. J. R. Meteorol. Soc.* **128**, 131–148.

Moorthi, S. and Suarez, M. 1992. Relaxed Arakawa–Schubert: a parametrization of moist convection for general circulation models. *Mon. Wea. Rev.* **120**, 978–1002.

Mureau, R., Molteni, F. and Palmer, T. N. 1993. Ensemble prediction using dynamically-conditioned perturbations. *Q. J. R. Meteorol. Soc.* **119**, 299–323.

Oortwijn, J. 1998. Predictability of the onset of blocking and strong zonal flow regimes. *J. Atmos. Sci.* **55**, 973–994.

Palmer, T. N., Gelaro, R., Barkmeijer, J. and Buizza, R. 1998. Singular vectors, metrics, and adaptive observations. *J. Atmos. Sci.* **55**, 633–653.

Puri, K., Barkmeijer J. and Palmer, T. N. 2001. Ensemble prediction of tropical cyclones using targeted diabatic singular vectors. *Q. J. R. Meteorol. Soc.* **127**(572), 709–731.

Smith, L. A. 2000. Disentangling uncertainty and error: on the predictability of non-linear systems. In: *Nonlinear Dynamics and Statistics* (ed. A. Mees). Birkhauser, Boston, 41–68.

Toth, Z. and Kalnay, E. 1997. Ensemble forecasting at NCEP and the breeding method. *Mon. Wea. Rev.* **125**, 3297–3319.

Tsuyuki, T. 1996. Variational data assimilation in the tropics using precipitation data. Part II: 3-D model. *Mon. Wea. Rev.* **124**, 2545–2561.

Tsuyuki, T. 1997. Variational data assimilation in the tropics using precipitation data. 3. Assimilation of SSM/I precipitation rates. *Mon. Wea. Rev.* **125**, 1447–1464.

Wang, Z. 1993. *Variational data assimilation with 2-D shallow water equations and 3-D FSU Global Spectral Models*. PhD Dissertation, Department of Mathematics, Florida State University, 235 pp.

Zeng, Q.-C. 1983. The evolution of a Rossby-wave package in a three-dimensional baroclinic atmosphere. *J. Atmos. Sci.* **40**, 73–86.

Zhu, Y. and Navon, I. M. 1997. Documentation of the tangent-linear and adjoint models of the radiation and boundary layer parametrization packages of the FSU Global Spectral Model T42L12. Technical Report, FSU-SCRI-97-98.

Zhu, Y. and Navon, I. M. 1999. Impact of parameter estimation on the performance of the FSU Global Spectral Model using its full-physics adjoint. *Mon. Wea. Rev.* **127**(7), 1497–1517.